Analysis of Qubit-Cavity System for Axion Detection Experiment

Marc Padilla Gandía[(1)], Jose R. Navarro Madrid[(1)], Alejandro Díaz Morcillo[(1)], David Díez Ibáñez[(2)]
marc.padilla@edu.upct.es, joser.navarro@upct.es, alejandro.diaz@upct.es, daviddiez@unizar.es
[(1)]Dpto. de Tecnologías de la Información y las Comunicaciones. Universidad Politécnica de Cartagena, 30202, Cartagena.
[(2)]Centro de Astropartículas y Física de Altas Energias (CAPA). Universidad de Zaragoza, 50009, Zaragoza.

***Abstract*—This article introduces the bases for the search of dark matter and the use of 3D transmon qubits, which will be used as single photon counters to improve the final sensitivity of the experiment. A system of two cavities and a qubit in between them is simulated, and the characteristics of the qubit are analyzed considering different sizes and positions for the multiple variables that define the geometry of the experiment. The objective of this work is to obtain a qubit-cavity system with ideal properties such as a high Purcell time, high coupling strengths and high quality factors for the cavities.**

I. Introduction

The hypothesis of Dark Matter was first introduced in the early 1930s based on the observation of galaxy clusters and the study of their properties [1]. With the discovery of the *Cosmic Microwave Background* it was highlighted the need for additional matter to exist beyond what was visible [2]. Many other scientific observations agree that a fraction of all matter in the universe must be non-baryonic and electrically neutral. This fraction was given the name of dark matter. Concretely the universe is thought to be composed approximately of 72% dark energy, 23% dark matter and finally 5% of baryonic matter.

One of the many proposed particles for dark matter is the axion. The axion, which is a very low mass particle, barely interact with ordinary matter [3]. In our universe axions could have been generated in two different situations: *before* the inflationary phase, generating axions with a mass lower than 25 µeV (6.045 GHz) whilst in the second case, *after* the inflationary phase of the universe, axions with a mass greater than 25 µeV would have been generated [4].

The detection of this particle can be done through the inverse Primakoff effect, which consist in the conversion of the axion into a photon under a very strong external magnetic field [5], with the mass of the axion being related to the frequency of the generated photon. Among several detection techniques to detect axions, the research of this paper is focused on haloscope experiments, whose aim is to search for axions present in our galaxy halo. Haloscope experiments are usually carried out on Earth´s surface as there is no immediate benefit from launching them to outer space.

One problem found is that the amount of noise that can be reduced is limited by the *Standard Quantum Limit* [6] since normally these experiments use Low Noise Amplifiers. A solution can be found by using single photon detectors, in this case a 3D transmon qubit. With the use of transmons a new limit in noise reduction can be achieved, as noise will be dominated by the Poisson fluctuations [6]. A transmon is a type of superconducting qubit. It's a modified version of the Cooper-pair box qubit, designed to have reduced sensitivity to charge noise while maintaining long coherence times, which are crucial for quantum operations [7].

II. The Cavities

The proposed detection setup is based on two cavities connected through a tiny iris in which the transmon will be placed as seen in Figure 1. The first is the *storage cavity*, where the axion-photon conversion is made and stored, whilst in the second one called *readout cavity* the qubit is interrogated to infer the population of the first cavity.

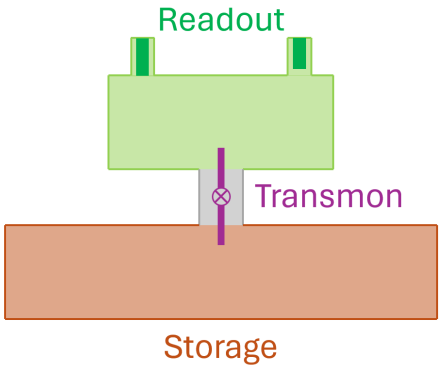

Fig. 1. System composed by two cavities and a qubit

One important parameter in the search for axions in a classical system is the detected power at the port, which can be written in natural units [8]:

$$P_d \approx g_{a\gamma}^2 \rho_{DM} \frac{1}{m_a} \kappa B_e^2 V Q_L C \tag{1}$$

where $g_{a\gamma}$ the unknown axion to photon coupling, ρ_{DM} the local dark matter density calculated to be around 0.3 to 0.4 GeV/cm^3 [9], κ the coupling factor, m_a the axion mass, B_e the strength of the external magnetic field, V the volume of the cavity, Q_L its loaded quality factor and C the form factor, which measures the coupling between the external magnetic field and the electric field generated by the axion-photon conversion. This parameter can be calculated as:

$$C = \frac{\left| \int_V \vec{E} \cdot \vec{B}_e dV \right|^2}{\int_V \left\| \vec{B}_e \right\|^2 dV \int_V \varepsilon_r \left\| \vec{E} \right\|^2 dV} \tag{2}$$

where ε_r is the relative electrical permittivity.

One of the objectives is to maximize the values of Q_L, V and C in order to improve the performance of the haloscope.

III. The Qubit

A qubit can be approximated as a two-level system, a ground state $|g\rangle$ and an excited state $|e\rangle$. This is achieved using a Josephson junction, which is a quantum device composed of two superconductors separated by a thin insulator, working as described by the two Josephson equations [10]:

$$I_s = I_c sin(\varphi) \tag{3}$$

$$\frac{d\varphi}{dt} = \frac{2\pi}{\Phi_0} V \tag{4}$$

where I_s is the supercurrent through the Josephson junction, I_c is the critical current of the superconductor, φ is the phase difference across the two superconductors, V is the externally applied voltage and Φ_0 is the magnetic flux quantum. Doing the time derivative of equation 3 and inserting the equation 4 we can obtain the following proportionality constant:

$$L_J = \frac{\Phi_0}{2\pi I_c cos(\varphi)} \tag{5}$$

which in the circuital sense implies a non-linear inductance. This component provides the non-linearity necessary for the qubit to work as an anharmonic oscillator [11].

Two important parameters are the Josephson energy E_J and the charging energy E_C which are calculated as:

$$E_J = \frac{\Phi_0 I_c}{2\pi} \tag{6}$$

$$E_C = \frac{e^2}{2C_J} \tag{7}$$

where e is the charge of the electron and C_J is the capacitance associated to the Josephson junction acting as a parallel plate capacitor. From these parameters we can extract the qubit frequency ω_q and the qubit anharmonicity α [11]:

$$\omega_q = \sqrt{8E_J E_C} - E_C \tag{8}$$

$$\alpha \approx -E_C \tag{9}$$

The qubit is not strictly a two-level system, but in this project only the subspace between the ground state $|g\rangle$ and the excited state $|e\rangle$ is used.

The complete qubit has a total capacitance of

$$C_\Sigma = C_G(C_S + C_J)/(C_G + C_S + C_J) \tag{10}$$

where C_G is the capacitance to ground and C_S the capacitance between the capacitive pads, which are added to allow coupling with the cavities.

In the axion detection operation, the qubit will be operated in the transmon regime, where $E_J/E_C \gg 1$, meaning the qubit will be insensitive to charge fluctuations which dephase it [11].

From the different functional parameters that characterize the qubit this work will focus on four of them:

- Qubit frequency (ω_q): resonant frequency at which the qubit can absorb or emit energy most efficiently.
- Coupling strengths (g): strength of interaction between the transmon qubit and the cavities.
- Purcell time (T_1): quantifies the timescale over which the qubit relaxes due to its interaction with the electromagnetic environment.
- Quality factors (Q_0): provides insight into the resonance characteristics, coherence properties, and interaction with its environment of the qubit and cavities.

Other parameters not discussed in this work are: qubit anharmonicity, charge dispersion and 2χ parameters.

In a real experiment, all these parameters, which model the behavior of the qubit-cavities system, will be measured by different techniques, as one-tone spectroscopy, two-tone spectroscopy, Rabi measurement, T1 measurement, and Ramsey measurement [12].

Comparative of classical LNA and single-photon detector

As stated before, single-photon detectors can surpass the Standard Quantum Limit of noise, but this is dependent on various factors, such as the temperature of the experiment T, the frequency, the detector quality factor Q_L and axion quality factor Q_a. The noise of both systems can be related as [13]:

$$[\frac{P_{LNA}}{P_{SPD}}] \approx \sqrt{\frac{Q_L}{2\pi Q_a} e^{hf/k_B T}} \tag{11}$$

where k_B is the Boltzmann´s constant and f the frequency. When this number is large, cavity photon counting can have a lower noise than linear detection.

IV. Simulation parameters

A parametric study in simulations has been performed with the following parameters: (see Figure 2)

- Length of the iris: l_{Iris}
- Length of the capacitive pads: l_p
- Position of the qubit from the center of the iris: p_q
- Length of the substrate containing the qubit: l_s

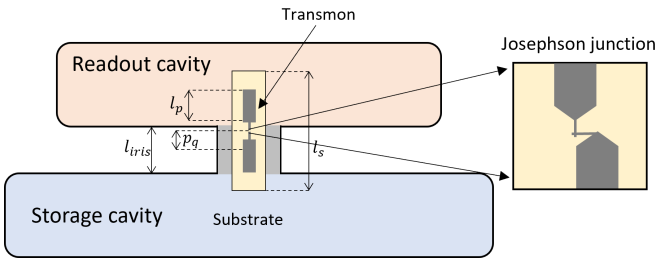

Fig. 2. Sketch of the system with the 4 analyzed parameters

From these parameters, information related to the qubit frequency, coupling strengths, Purcell time and quality factors has been extracted.

The simulations have been performed using *CST Studio Suite* [14] software, and the data has been studied using *Python* programming language, implementing the Black-Box formulation [15], where the resonances of the linear system are first identified and then the nonlinearity of the Josephson junction is introduced according to the equation

$$Y(\omega) = j\omega C_J - \frac{j}{\omega L_J} + Y_c(\omega) \tag{12}$$

where C_J and L_J are the Josephson capacitance and inductance, respectively, and $Y_c(\omega)$ is the admittance of the system without the junction. From this parameter the resonance

frequencies can be obtained for the qubit and both cavities as seen in Figure 3.

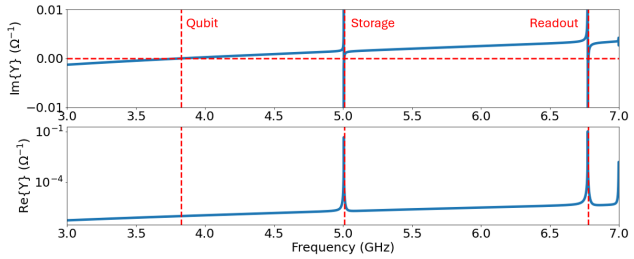

Fig. 3. Admittance $Y(\omega)$ and the three resonances: qubit, storage, and readout

By manipulating the real and imaginary parts of the admittance, multiple parameters can be obtained. Furthermore, using creation and destruction operators, the eigenstates of the whole system can be obtained from which other important parameters are calculated. This is performed creating a quantum object called $\hat{a}$ for each resonance through the tensor product of destruction operators and Hilbert spaces, and using it to calculate the final Hamiltonian of the system [15]. Through this Hamiltonian the resonances of the whole system are calculated from which multiple important parameters are obtained: self-Kerr and cross-Kerr shift $2\chi_{qp}$, effective resonant vacuum Rabi rate or coupling strength g_p and Purcell time T_1. These two last parameters equations are:

$$g_p = \sqrt{\chi_{qp}\Delta_{qp}\frac{\Delta_{qp}+\alpha_q}{\alpha_q}} \tag{13}$$

$$T_1 = \frac{1}{(\frac{g_r}{f_r-f_q})^2\frac{2\pi f_r 10^9}{Q_r}} \tag{14}$$

where Δ_{qp} is the difference between the qubit frequency and the mode p, g_r, f_r and Q_r are the coupling strength, frequency and quality factor of the readout cavity respectively, and f_q the frequency of the qubit.

V. Results and Discussion

A. Length of the iris

The first parameter to be analyzed is the length of the iris, which can be defined as the separation between storage and readout cavity. As the length of the iris increases less part of the capacitive pads protrude into the cavities, diminishing the coupling strengths of both cavities as seen in Figure 4. A consequence of this is an increase in the Purcell time. The frequencies and Qs of the cavities stay almost the same as they are only getting further away one from the other. Although a bigger T_1 makes the measurements easier, the decrease in the coupling strengths makes them more difficult.

B. Length of the capacitive pads

Another parameter is the size of the capacitive pads used to couple the qubit with the cavities. With the increase in area of the capacitive pads, the coupling strengths also increase as observed in Figure 6. This causes a decrease in the Purcell time seen in Figure 7 and in the quality factors of the cavities in Figure 8. This implies the qubit will relax faster as the pads area increases, making measurements more complicated.

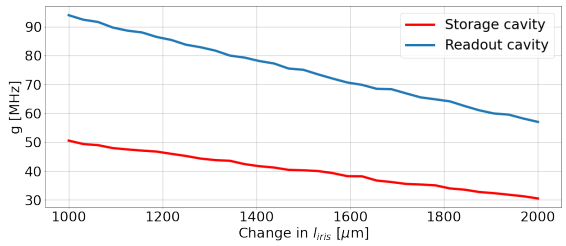

Fig. 4. Coupling strength of the readout and storage cavities versus length of the iris

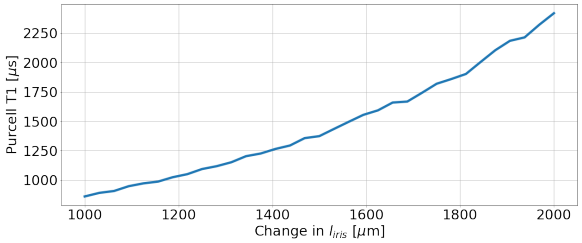

Fig. 5. Purcell time versus length of the iris

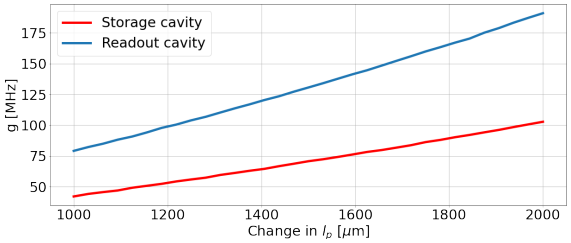

Fig. 6. Coupling strength of the cavities versus length of the pads

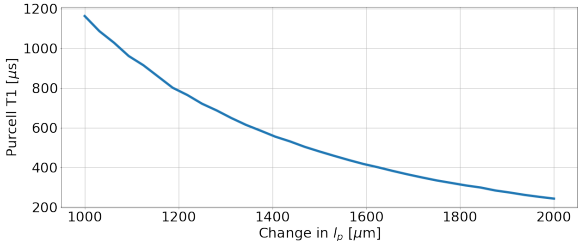

Fig. 7. Purcell time versus length of the pads

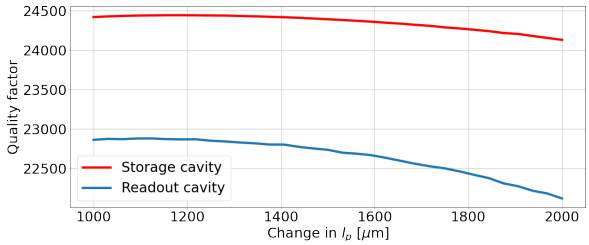

Fig. 8. Quality factors of the cavities versus length of the pads

C. Position of the qubit

In this subsection the position of the qubit in relation to the center of the iris is analyzed dividing it into two cases:

1) Protrusion into storage cavity: As the qubit moves further into the storage cavity the coupling strength of this cavity increases while the coupling strength to the readout cavity decreases. The quality factor of the opposite cavity falls rapidly once the qubit is fully immersed in the cavity.

2) Protrusion into readout cavity: In this other case the opposite happens, as the qubit is inserted into the readout cavity the coupling strength to this cavity becomes greater at the cost of the coupling to the storage cavity. This also implies a sharp fall in the Purcell time as the qubit is inserted into the readout cavity (see Figure 9). As in the first case the opposite cavity quality factor decreases dramatically the moment the qubit is inside the cavity. This phenomenon can be seen in Figure 10 where the negative part of the x-axis represents the qubit being inserted into the storage cavity and the positive part towards the readout cavity.

Combining both results it can be concluded the positioning of the qubit is key to avoid the quality factors from falling and worsening the figure of merit of the axion search.

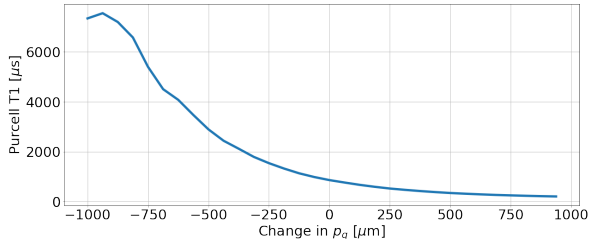

Fig. 9. Purcell time versus position of the qubit

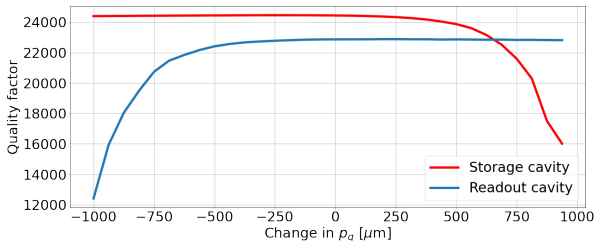

Fig. 10. Quality factor of the cavities versus position of the qubit

D. Length of the substrate

Here, two models were compared, one with a short substrate and another one with a long substrate. The objective was to analyze the influence of the substrate inside the cavities in the value of Q_0 and C. It was found that the presence of extra substrate in the storage cavity barely made an impact into the cavity form factors or the quality factors, meaning a longer substrate could be used to provide extra support to the qubit. The only noticeable change occurred in the coupling strength of the storage cavity, increasing with the presence of extra substrate inside the cavity.

VI. Conclusions

Multiple qubit-cavity system simulations have been performed and their properties have been studied, showing the quality factors of the cavities remain the same, independent from the qubit parameters except for the position of the qubit which is critical to ensure a good quality factor. Furthermore, a trade-off is found between coupling strength of the readout cavity and the Purcell time, meaning these two parameters cannot be maximum at the same time.

Acknowledgements

This work was realized within the RADES group; authors thank our colleagues for their support, specially Akash V. Dixit for providing most part of the black-box quantization script. It has been funded by MCIN/AEI/10.13039/501100011033/ and by "ERDF A way of making Europe", under grants PID2019-108122GB-C33, PID2022-137268NB-C53. Marc Padilla and Alejandro Díaz thank Fundación Avanza and its support under the DACIU program.

References

[1] Zwicky, F. Die Rotverschiebung von extragalaktischen Nebeln. *Helv. Phys. Acta*. **6** pp. 110-127 (1933)

[2] Dicke, R., Peebles, P., Roll, P. & Wilkinson, D. Cosmic Black-Body Radiation. *Astrophys. J.*. **142** pp. 414-419 (1965)

[3] Adams, C. et al. Axion Dark Matter. *Snowmass 2021*. (2022,3)

[4] Workman, R. et al. Review of Particle Physics. *PTEP*. **2022** pp. 083C01 (2022)

[5] Primakoff, H. Photo-Production of Neutral Mesons in Nuclear Electric Fields and the Mean Life of the Neutral Meson. *Phys. Rev.*. **81**, 899-899 (1951,3)

[6] Lamoreaux, S., Bibber, K., Lehnert, K. & Carosi, G. Analysis of single-photon and linear amplifier detectors for microwave cavity dark matter axion searches. *Phys. Rev. D*. **88**, 035020 (2013)

[7] Devoret, M. & R. J. Schoelkopf Superconducting Circuits for Quantum Information: An Outlook. *Science*. **339**, 1169-1174 (2013)

[8] Díaz-Morcillo, A. et al. Design of New Resonant Haloscopes in the Search for the Dark Matter Axion: A Review of the First Steps in the RADES Collaboration. *Universe*. **8**, 5 (2021)

[9] Salas, P., Malhan, K., Freese, K., Hattori, K. & Valluri, M. On the estimation of the Local Dark Matter Density using the rotation curve of the Milky Way. *JCAP*. **10** pp. 037 (2019)

[10] Josephson, B. The discovery of tunnelling supercurrents. *Rev. Mod. Phys.*. **46** pp. 251-254 (1974)

[11] V. Dixit, A. Searching for dark matter with superconducting qubits. (2021)

[12] Naghiloo, M. Introduction to Experimental Quantum Measurement with Superconducting Qubits. (2019)

[13] Lamoreaux, S., Bibber, K., Lehnert, K. & Carosi, G. Analysis of single-photon and linear amplifier detectors for microwave cavity dark matter axion searches. *Phys. Rev. D*. **88**, 035020 (2013)

[14] https://www.3ds.com/products/simulia/cst-studio-suite

[15] Nigg, S. et al. Black-Box Superconducting Circuit Quantization. *Phys. Rev. Lett.*. **108**, 240502 (2012)